TRANSPORT OF CHEMICAL SPECIES FROM THE TROPOSPHERE TO THE STRATOSPHERE BY DEEP CONVECTIVE CLOUDS

Pao K. Wang

Department of Atmospheric and Oceanic Sciences, University of Wisconsin-Madison
Madison, WI 53706, USA

ABSTRACT

Satellite and aircraft observations have shown the existence of cirrus plumes above the anvils of some severe thunderstorms. Simulations of thunderstorms using a cloud resolving model reproduce these plumes well. Analysis of the model results shows that the source of moisture for the plumes is in the storm below. This indicates a cross-tropopause transport of water vapor from the troposphere to the stratosphere. This further implies that other chemical species, especially those relatively inert ones, can be transported likewise. Some observational evidence and model results will be presented and possibilities of observation by SOFIA will be discussed.

INTRODUCTION

Water vapor is important to the radiative budget of the atmosphere, and hence to climate studies, because of its strong absorption of infrared (IR) radiation. It is also the main source of ozone-destroying HO_x radicals in the lower stratosphere. In the condensed phase, as exemplified by the recently observed anvil-top plumes (*Setvak and Doswell*, 1991*; Levizzani and Setvak*, 1996) to be discussed in detail later, it serves as a catalytic surface for heterogeneous reactions involving NO_x and halogen species (e.g., *Solomon*, 1999). It is clear that the distribution of water substance in the upper troposphere/lower stratosphere (UT/LS) region has significant impacts on the global climate process.

If the stratospheric water vapor concentration is not steady-state, then its implications for climatic change must be carefully considered. A recent finding by *Oltmans et al.* (2000), using balloon-borne frostpoint hygrometers, shows that the stratospheric water vapor concentrations measured at two midlatitude locations (Washington, DC and Boulder, Colorado) have increased by 1-1.5% yr^{-1} for the past 35 years, making the climatic impact of stratospheric water vapor even more likely. The distribution of water vapor in the UT/LS is of special interest because this region is strongly influenced by the dynamics of stratospheric-tropospheric exchange, both diabatically and adiabatically, and may be chemically perturbed by subsonic aircraft emissions (*Pan et al.*, 1997).

Using water vapor data from the Stratospheric Photochemistry, Aerosols and Dynamics Expedition (SPADE), *Hintsa et al.* (1994) found higher water vapor concentration in the NH in fall than in spring. *Pan et al.* (1997), using Stratospheric Aerosol and Gas Experiment II (SAGE II) data, found a strong seasonal cycle of the water vapor mixing ratio on the 320K isentropic surface for both hemispheres, with maximum values in summer and minimum values in early spring. By also analyzing SAGE II ozone data, they inferred from both water vapor and ozone data that extratropical UT/LS exchange has a significant influence on the lowermost stratosphere, especially in the NH summer season. There are others who also contributed significantly to the research of stratospheric water vapor.

The transport mechanisms discussed so far appear to be all large-scale in nature. It is desirable to understand these transport mechanisms in smaller scale so that finer physical processes involved can be identified. Understanding these processes in smaller scale not only helps to clarify the transport mechanisms, but also provides conceptual basis for in situ aircraft measurements. Furthermore, such knowledge will afford modelers to perform quantitative computations so as to obtain more accurate estimates and better transport parameterizations for global models.

The paper proposes a cloud-scale mechanism that can transport atmospheric constituents (including water vapor) from the troposphere to the stratosphere. Unlike the studies of both *Dunkerton* (1995) and *Chen* (1995), both of which concern adiabatic (isentropic) transport, this is a diabatic mechanism that is associated with the breaking of gravity waves at the tops of deep convective storms in the middle latitudes. To illustrate this mechanism, a three-dimensional cloud dynamical model with detailed cloud microphysics package was utilized to perform a simulation study of a typical High Plains supercell storm. The model results are used to demonstrate this transport process.

OBSERVATIONAL EVIDENCE OF ANVIL TOP PLUMES

Fig. 1 shows a composite of channels 1, 2, and 4 GOES satellite image of a line of thunderstorms in the Plains of US. The cirrus plume is clearly visible about the thunderstorm cell near Texas-Oklahoma border region. It is the features like this that motivated this study.
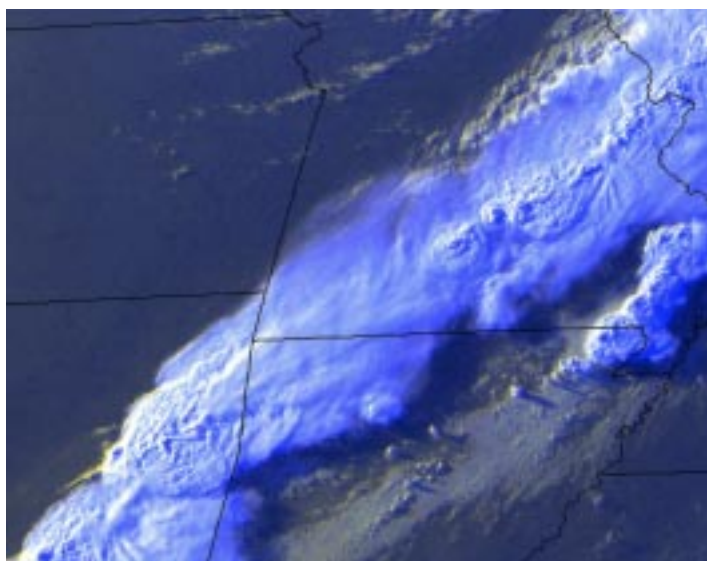

Fig. 1: GOES satellite image.

THE CLOUD MODEL AND THE CCOPE SUPERCELL

The tool utilized for the present study is the Wisconsin Dynamical/Microphysical Model (WISCDYMM), which is a three-dimensional, quasi-compressible, time-dependent, non-hydrostatic primitive-equation cloud model developed at the University of Wisconsin-Madison by the author's research group. More detailed descriptions of the model can be found in Straka (1989) and Johnson et al. (1993, 1994). The results reported here are based on the medium resolution (1 x 1 x 0.2 km) runs

The storm chosen for the simulation for illustrating the plume-formation mechanism is a supercell that passed through the center of the Cooperative Convective Precipitation Experiment (CCOPE) (see *Knight*, 1982) observational network in southeastern Montana on 2 August 1981.

RESULTS AND DISCUSSIONS

Central Cross-section Features

In the following discussions, the plume phenomenon in the simulated storm will be illustrated first using the fields of *relative humidity with respect to ice saturation*, RHi, which is more relevant than the relative humidity with respect to liquid water, because ice is far more common at the cloud top temperatures.

The simulation results reveal that there are at least two different plume formation processes at the cloud top. The first, associated with the overshooting dome of the storm, will be called the "overshooting plume" for convenience. The second, associated with the breakaway of cloud top materials in the anvil sheet downstream from the updraft core, will be called the "anvil sheet plume" to distinguish it from the overshooting plume. In the present simulation the anvil sheet plume occurs earlier than the overshooting plume, but this order is not necessarily a rule, as it probably depends on the circumstances. As we will see later, both types of plumes are caused by the breaking of cloud top gravity waves.

Figure 2 shows six snapshots of the RHi profiles in the central east-west cross-section (y = 27 km) of the storm. This is where the storm development is normally (though not always) most vigorous. Since the cloud top region is the focus here, these snapshots are windowed to 10-20 km vertically and 20-55 km horizontally, with the vertical scale stretched in these views. Note also that all descriptions of distances and directions in the following discussions are storm-relative. During the computation, the simulated storm is moving east as did the actual CCOPE storm. In order to keep the storm in the computational domain, the mean storm motion has been subtracted from the wind field so that the simulated storm appears to be quasi-stationary in the resulting reference frame.

No obvious plume structure is discernible before 24 min into the simulated storm activity. At 24 min, as shown in the first panel in Fig. 2, strong gravity wave motions at the cloud top are visible. There is a large surge of comparatively high humidity (RHi ~ 30-50%) above the second wave crest (to the east of the main updraft column) that seems to propagate upward and westward (i.e., upstream relative to the upper-level wind direction) into the stratosphere. At 32 min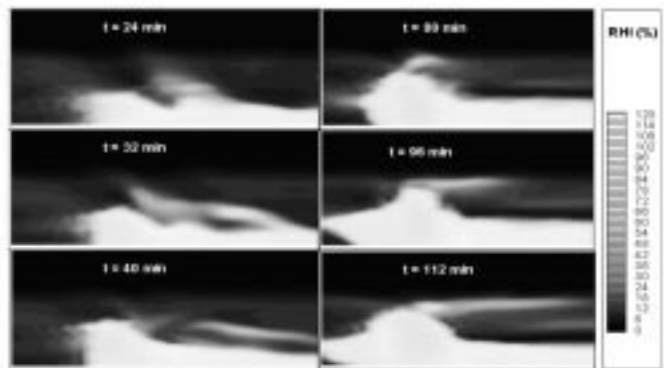, this moist surge appears to be nearly detached from the anvil of the storm and form a separate moist layer in the stratosphere. The surge appears to consist of two parts, one to the west and one to the east. The one to the west (left) is less humid (RHi ~ 40%) and seems to merge with the overshooting dome later while the one to the east (right, RHi~50-75%) becomes slightly elevated and develops into a separate plume above the storm anvil at 40 min. This plume, sloping slightly downward toward the downstream direction and almost parallel to the slope of the anvil, appears to gradually dissipate with time into a diffuse moist layer. Relative to the storm, the anvil sheet plume seems to propagate upstream, and may be responsible for the formation of the stratospheric cirrus as observed by

Fig. 2: Snapshots of vertical RHi (relative humidity with respect to ice) profiles at t = 24, 32, 40, 80, 96, and 112 min in the central east-west cross-section (y = 27 km), showing the plume feature above the anvil. Only the portion near the cloud top is shown. The vertical axis range is 10-20 km and horizontal axis range 20-55 km.

Fujita (1982), who stated that "One of the most striking features seen repeatedly above the anvil top is the formation of cirrus cloud which jumps upward from behind the overshooting dome as it collapses violently into the anvil cloud". The animation of plume formation at this stage matches this description very well.

Another stage of plume formation, the overshooting plume, starts at about 80 min into the simulation, as shown by the three snapshots on the right-hand-side in Fig. 2. The RHi of the overshooting plume is generally much higher than that of the anvil sheet plume. At 80 min, a moist patch appears to emanate from the overshooting dome. Subsequently, it gradually takes on the shape of a chimney plume. The stretching of the plume downwind is apparently caused by the upper-level winds, which are predominantly westerlies. The maximum RHi in the core of the plume sometimes exceeds 100%. At 112 min, the plume has reached the east boundary of the computational domain and an altitude of 15-16 km.

The altitude of the anvil sheet plume, in contrast, is 12 -13 km. Thus there may be more than one layer of plumes at a given time. The precise thickness of plumes depends on the choice of RHi that defines their boundaries, but generally the thickness ranges from several hundred meters to about 1 km for RHi ≥10%. It is also seen from the figure that there is a shallow dry layer immediately above the anvil. This layer is about 1-1.5 km thick and apparently extends to the whole length of the anvil in the computational domain.

3-D Cloud Top Features

The discussions in the previous section are based on the plume features shown in the central vertical cross-sections of the storm. The single cross-sectio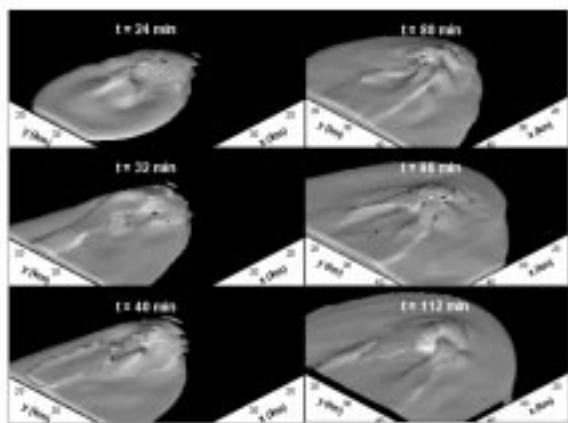nal view obviously does not reveal the three-dimensional structure of the plume, which is shown in Fig. 3. Here again, only the portion of the storm above 10 km is shown. Six snapshots of the cloud tops, represented here by the contour surface of RHi = 30%, are shown as seen from above and northeast of the storm. The value 30% is chosen so that the physical characteristics of the plumes can be clearly examined. A choice of surfaces at a higher RHi value results in somewhat smaller plume whereas choosing a smaller RHi value results in somewhat larger plumes, but the main characteristics remain very much the same.

Fig. 3. Snapshots of 3D renderings of the 30% RHi contour surface at t = 24, 32, 40, 80, 96, and 112 min showing the plume features above the anvil. Data below 10 km are clipped.

As in Fig. 1, the plume associated with the second wave crest becomes noticeable at t = 24 min. At t = 32 min, this plume becomes larger and moves both upward and upstream. It then recedes downstream afterward, as revealed by the image at t = 40 min, gradually dissipates, and becomes nearly invisible after 60 min. On the other hand, the plume associated with the overshooting top first become recognizable at 36 min at a level above the wave-crest plume. It fluctuates in size for a while, but becomes elongated into a chimney plume shape starting at 80 min. The main orientation is along the upper-level wind, although there are slight meanders, probably due to the perturbation of the flow passing the overshooting dome.

The snapshots at 80, 96, and 112 min also show that there is another plume-like structure at a lower level of the overshooting dome. It seems to emanate from a mid-level point and orient northeast in the beginning. This lower level plume is sometimes separated from the anvil below, although it eventually merges with the latter. Obviously, this side-protruding plume would not be revealed in the central cross-sections.

More details of the descriptions of the model results are given in Wang (2003).

MECHANISM OF PLUME FORMATION

Wang (2003) has given more detailed discussions on the formation mechanisms of such plumes. It is the gravity wave breaking that is responsible for the irreversible transport of moisture across the tropopause. The same mechanism will also transport other trace species (trace gases, aerosol particles) and may contribute to the formation of the Junge aerosol layer. This is demonstrated by a simulation of the same storm with embedded inert tracer and the results will be reported elsewhere.

OBSERVATIONAL POSSIBILITIES BY SOFIA

So far most observational evidence were either from satellites which see water plumes or a few aircraft indirect observations (such as Fujita's "jumping cirrus"). There is a lack of direct measurements of either water vapor or other trace chemicals (gases or particulates). It appears that SOFIA should be able to contribute to the measurements of these species and verify the tropospheric contributions to the chemistry of the stratosphere via deep convective storms.

REFERENCES

Chen, Ping, Isentropic cross-tropopause mass exchange in the extratropics. *J. Geophys. Res*., **100**, 16661-16673, 1995.

Dunkerton, T. J., Evidence of meridional motion in the summer lower stratosphere adjacent to monsoon regions. *J. Geophys. Res*., **100**, 16675-16688, 1995.

Hintsa, E. J., E. M. Weinstock, A. E. Dessler, J. G. Anderson, M. Lowenstein, and J. R. Podolske, SPADE H2O measurements and the seasonal cycle of stratospheric water vapor. *Geophys. Res. Lett.*, **21**, 2559-2562, 1994.

Knight, C. A., Ed., The Cooperative Convective Precipitation Experiment (CCOPE), 18 May-7 August 1981. *Bull. Amer. Meteor. Soc*., **63**, 386-398, 1982.

LevizzaniV., and M. Setvak, Multispectral, high resolution satellite observations of plumes on top of convective storms*. J. Atmos. Sci*., **53**, 361-369, 1996.

Oltmans, S. J., H. Volmer, D. J. Hofman, K. H. Rosenlof, and D. Kley, The increase in stratospheric water vapor from balloonborne, frostpoint hygrometer measurements at Washington, D. C., and Boulder, Colorado. *Geophys. Res. Lett*., **27**, 3453-3456, 2000.

Pan, L., S. Soloman, W. Randel, J-F. Larmarque, P. Hess, J. Gille, E. Chiou, and M. P. McCormick, Hemispheric symmetries and seasonal variations of the lowermost stratospheric water vapor and ozone derived from SAGE II data. *J. Geophys. Res*., **102**, 28177-28184, 1997.

Pan, L. L., E. J. Hinsta, E. M. Stone, E. M. Weinstock, and W. J. Randel, The seasonal cycle of water vapor and saturation vapor mixing ratio in the extratropical lowest stratosphere. *J. Geophys. Res*., **105**, 26519-26530, 2000.

Setvak, M. and C. A. Doswell III, The AVHRR channel 3 cloud top reflectivity of convective storms. *Mon. Wea. Rev*., **119**, 841-847, 1991.

Solomon, S., Stratospheric ozone depletion: A review of concept and history. *Rev. Geophys*.,**37**, 275-316, 1999.

Straka, J. M., *Hail growth in a highly glaciated central high plains multi-cellular hailstorm.* Ph.D thesis, UW-Madison, 1989.

Wang, P. K., Moisture Plumes above Thunderstorm Anvils and Their Contributions to Cross Tropopause Transport of Water Vapor in Midlatitudes. *J. Geophys. Res.*, **108**[D6], 4194, doi: 10.1029/2003JD002581, 2003.